

RESEARCH ARTICLE

Translational Physiology

## The novel STING antagonist H151 ameliorates cisplatin-induced acute kidney injury and mitochondrial dysfunction

Wei Gong,<sup>1,2,3\*</sup> Lingling Lu,<sup>1,2,3\*</sup> Yu Zhou,<sup>1,2,3\*</sup> Jiaye Liu,<sup>1,2,3</sup> Haoyang Ma,<sup>1,2,3</sup> Lvhan Fu,<sup>1,2,3</sup> Songming Huang,<sup>1,2,3</sup> Yue Zhang,<sup>1,2,3</sup> Aihua Zhang,<sup>1,2,3\*</sup> and Zhanjun Jia<sup>1,2,3\*</sup>

<sup>1</sup>Nanjing Key Lab of Pediatrics, Children's Hospital of Nanjing Medical University, Nanjing, China; <sup>2</sup>Jiangsu Key Laboratory of Pediatrics, Nanjing Medical University, Nanjing, China; and <sup>3</sup>Department of Nephrology, State Key Laboratory of Reproductive Medicine, Children's Hospital of Nanjing Medical University, Nanjing, China

### Abstract

Stimulator of interferon genes (STING) is an important adaptor in cytosolic DNA-sensing pathways. A recent study found that the deletion of STING ameliorated cisplatin-induced acute kidney injury (AKI), suggesting that STING could serve as a potential target for AKI therapy. Up to now, a series of small-molecule STING inhibitors/antagonists have been identified. However, none of the research was performed to explore the role of human STING inhibitors in AKI. Here, we investigated the effect of a newly generated covalent antagonist, H151, which targets both human and murine STING, in cisplatin-induced AKI. We found that H151 treatment significantly ameliorated cisplatin-induced kidney injury as shown by the improvement of renal function, kidney morphology, and renal inflammation. In addition, tubular cell apoptosis and increased renal tubular injury marker neutrophil gelatinase-associated lipocalin induced by cisplatin were also effectively attenuated in H151-treated mice. Moreover, the mitochondrial injury caused by cisplatin was also reversed as evidenced by improved mitochondrial morphology, restored mitochondrial DNA content, and reversed mitochondrial gene expression. Finally, we observed enhanced mitochondrial DNA levels in the plasma of patients receiving platinum-based chemotherapy compared with healthy controls, which could potentially activate STING signaling. Taken together, these findings suggested that H151 could be a potential therapeutic agent for treating AKI possibly through inhibiting STING-mediated inflammation and mitochondrial injury.

**NEW & NOTEWORTHY** Although various stimulator of interferon genes (STING) inhibitors have been identified, no research was performed to investigate the role of human STING inhibitors in AKI. Here, we evaluated the effect of H151 targeting both human and murine STING on cisplatin-induced AKI and observed a protection against renal injury possibly through ameliorating inflammation and mitochondrial dysfunction.

*acute kidney injury; cisplatin; H151; mitochondrial dysfunction; stimulator of interferon genes*

### INTRODUCTION

Acute kidney injury (AKI) comprises a group of clinical syndromes characterized by the sudden or continued decrease of renal function as shown by rapidly increased serum creatinine and reduced estimated glomerular filtration rates (1). AKI usually happens in hospitalized patients with high morbidity and mortality. According to data in clinical observations, a 2–7% incidence of AKI occurred in hospitalized patients, and the mortality in patients in the intensive care unit was up to 50% (2). More seriously, surviving patients of AKI have higher risks of progressing into chronic kidney disease and end-stage renal disease compared with patients

without AKI (3), bringing heavy burdens to families and society. However, specific and satisfactory therapies for AKI are still absent because of the incomplete understanding of the complex pathogenesis.

Recently, a study from Maekawa et al. (4) demonstrated that the cytosolic DNA-sensing adaptor stimulator of interferon genes (STING) participated in AKI and regulated tubular inflammation. STING is an important adaptor in the cytosolic DNA-induced signaling pathway. In brief, cytosolic double-strain (ds)DNA, which is mainly pathogen-derived dsDNA or cyclic self-DNA, could be recognized by cyclic cGMP–AMP synthase and then catalyzed to cGAMP. Binding of cGAMP activates STING, which then translocates to the

\* W. Gong, L. Lu, and Y. Zhou contributed equally to this work; A. Zhang and Z. Jia contributed equally to this work.

Correspondence: Z. Jia (jiazj72@hotmail.com).

Submitted 20 October 2020 / Revised 3 February 2021 / Accepted 15 February 2021



Golgi and activates TANK-binding kinase 1 (TBK1). TBK1 then phosphorylates transcriptional factors including interferon regulatory factor 3 and NF- $\kappa$ B, which initiate the transcription of innate immune genes and inflammatory factors (5–8). Besides exogenous DNA and endogenous nuclear DNA, DNA from damaged mitochondria is also a trigger for activity of the STING signaling pathway (9–11).

Up to now, STING activity has been reported to be involved in many pathological events, including host defense against infection, tumor, inflammation, autoimmune, and diseases (12–16). Moreover, targeting STING is considered as a potentially effective strategy for the treatment of inflammation-associated diseases, such as AKI, sepsis, colitis, and nonalcoholic steatohepatitis (4, 11, 17, 18). H151 is a covalent small molecule inhibiting STING palmitoylation and thus blocking STING-mediated signaling pathways. H151 was identified as a more advanced antagonist targeting human STING than other related derivatives such as C-176, as H151 had a highly potent and selective inhibitory effect on human STING. Interestingly, H151 also dramatically inhibited STING activity in mice (19), which provided the opportunity to test the effect of H151 in mouse models. However, none of researches has been performed to explore the role of human STING inhibitors including H151 in experimental models *in vivo*. Here, we investigated the effect of H151 using a mouse model of AKI induced by cisplatin. Our results suggested that H151 could strikingly ameliorate cisplatin-induced renal dysfunction, tubular injury, renal inflammation, and mitochondrial dysfunction. These findings suggested that H151 could serve as a potential therapeutic agent for AKI.

## MATERIALS AND METHODS

### Patients and Study Approval

Blood samples from patients with tumor who were undergoing diagnostic evaluation in the Affiliated Hospital of Nanjing Medical University (Nanjing, China) and treated with platinum-based chemotherapy were collected for the analysis of plasma mtDNA. The information of patients is shown in Table 1. The agreement describing the use of human samples and the clinical information in this study was approved by the Human Subjects Committee of Nanjing Medical University. Informed consent was obtained from all participants.

### Plasma mtDNA Isolation and Assessment

Blood samples were collected into EDTA-containing tubes and centrifuged initially at 3,000 rpm for 10 min. The

plasma was separated and centrifuged for another 10 min at 10,000 rpm to obtain cell-free plasma. Whole DNA in plasma was isolated using the QIAamp DNA Blood Midi kit (Qiagen, Valencia, CA) following the manufacturer's instructions.

mtDNA in the whole DNA from plasma was assessed using quantitative real-time PCR (qRT-PCR). Mitochondrial genomic regions of mitochondrially encoded NADH:ubiquinone oxidoreductase core subunit 1 (mt-ND1), mitochondrially encoded cytochrome *c* oxidase III (mt-CO3), and mitochondrially encoded cytochrome *b* (mt-CYTB) were selected to quantify mtDNA levels. mtDNA was expressed as threshold cycle ( $C_t$ ) values as previously described (20); higher  $C_t$  values indicated lower levels of mtDNA in plasma.

### Animals

Pathogen-free, male C57BL/6J mice (8–10 wk) were purchased from GemPharmatech (Nanjing, China). All mice were maintained under standard environmental conditions at 19–21°C on a 12:12-h light-dark cycle. They were allowed free access to drinking water and a standard rodent diet. All experiments in animals were in accordance with guidelines approved by the Institutional Animal Care and Use Committee of Nanjing Medical University (IACUC 14030112-2).

### Animal Experiments

Mice were randomly assigned to the following three groups: the control group and cisplatin-induced groups with or without H151 (Cat. No. HY-112693, MedChemExpress) treatment. A single intraperitoneal injection of cisplatin was used to induce AKI at a dose of 25 mg/kg. H151 [7 mg/kg/day, according to the previous study (19)] was administered intraperitoneally to the mice at 1 h before cisplatin injection and continually administration at the same time every day after cisplatin treatment. Seventy-two hours after the cisplatin injection, all mice were euthanized, and blood samples and kidney tissues were collected. Cross sections of the left kidneys were fixed in 4% paraformaldehyde for histological examination, and the rest of the kidney tissue was immediately frozen in liquid nitrogen and stored at –80°C. Concentrations of blood urea nitrogen (BUN) and creatinine were measured by a serum biochemical autoanalyzer at the biochemistry laboratory of Nanjing Children's Hospital. In a separate experiment, mice in the same conditions were monitored for survival.

### Immunohistochemistry

Mouse STING immunohistochemistry staining was performed in paraffin-embedded renal tissues according to previously described methods (21). After treatment, sections

**Table 1.** General data of the patients

Sex	Age, yr	Pathological Diagnosis	Platinum-Based Chemotherapy Drug
Male	44	Nasopharyngeal carcinoma	Cisplatin
Female	44	Cervical carcinoma	Nedaplatin
Female	52	Cervical carcinoma	Carboplatin
Male	15	Nasopharyngeal carcinoma	Nedaplatin
Female	65	Cholangiocarcinoma	Oxaliplatin
Male	62	Small cell lung carcinoma	Cisplatin
Female	46	Cervical carcinoma	Cisplatin
Female	45	Cervical carcinoma	Cisplatin

were incubated with anti-STING antibody (Cat. No. 19851-1-AP, Proteintech, Wuhan, China) overnight at 4°C. Color reaction was performed using diaminobenzidine and visualized using microscopy.

### Histological Analysis

Sections (3 µm) that were embedded in paraffin were stained with hematoxylin and eosin. A pathologist analyzed these sections in a blind manner. A minimum of five fields at ×200 magnification for each kidney were examined and scored for tubular injury. Histopathological changes were evaluated by the percentage of renal tubules that displayed cell lysis, loss of the brush border, and cast formation. Each sample was scored from 0 to 4, where 0 = no abnormalities; 1+ = <25%, 2+ = 25%–50%, 3+ = 50%–75%, and 4+ = >75% (22). The average histological score for each sample was calculated.

### Transmission Electron Microscopy

Mitochondrial structures of renal tubular cells were examined by standard transmission electron microscopy as previously

described (23). Ultrathin sections were observed in a transmission electron microscope (JEOL JEM-1010, Tokyo, Japan).

### RNA Isolation and qRT-PCR Analysis

Total RNA from kidney tissues was extracted by RNAiso reagent (Cat. No. 9108, Takara Bio, Dalian, China) following the manufacturer's instructions. Quantitative real-time PCR was performed to detect target gene expression using an ABI 7300 Real-Time PCR Detection System with SYBR Green PCR Master Mix (Cat. No. q111-02/03, Vazyme, Nanjing, China). The cycling conditions were 95°C for 10 min followed by 40 repeats of 95°C for 15 s and 60°C for 1 min. Relative amounts of mRNA were calculated using the  $\Delta C_t$  method as normalized to the GAPDH control or normalized to 18S in the analysis of mitochondrial genome-encoded gene expression. The sequences of the primers are shown in Table 2.

### Mitochondrial Genome Quantification

Total DNA of renal tissues was extracted using a DNA Extraction kit obtained from TIANGEN (Beijing, China).

**Table 2.** Primer sequences for quantitative RT-PCR

Gene Symbol	Primer Sequences (5'–3')	Official Full Name
<i>Murine</i>		
mt-ND1	F: ACACCTATTACAACCAAGAACACAT R: TCATATTATGGCTATGGGTCAGG	NADH dehydrogenase 1, mitochondrial
mt-ND2	F: CCATCAACTCAATCTCACTTCTATG R: GAATCCTGTAGTGGTGGAAGG	NADH dehydrogenase 2, mitochondrial
mt-ND4	F: GCTTACGCCAAACAGAT R: TAGGCAGAAATAGGAGTGAT	NADH dehydrogenase 4, mitochondrial
mt-CO1	F: CAGACCGCAACCTAAACACA R: TTCTGGGTGCCCAAGAAT	Cytochrome c oxidase I, mitochondrial
mt-CO2	F: GCCGACTAAATCAAGCAACA R: CAATGGGCATAAAGCTATGG	Cytochrome c oxidase II, mitochondrial
mt-CO3	F: CGTGAAGGAACCTACCAAGG R: ATTCTGTGGAGGTGCGACA	Cytochrome c oxidase III, mitochondrial
mt-ATP6	F: CCATAAATCTAAGTATAGCCATTCCAC R: AGCTTTTGTAGTTTGTGTCGGAAG	ATP synthase 6, mitochondrial
mt-CYTB	F: GAGGTTGGTTCGGTTTTGG R: GTTTTGAAAGGGTGGGTGAC	Cytochrome b, mitochondrial
Chr6	F: ATGGAAAGCCTGCCATCATG R: TCCTTGTGTTCAGCATCAC	Mouse chromosome 6
18S rRNA	F: TTCGGAAGTGAAGCCATGATT R: TTTTCGCTCTGGTCCGTCTTG	18S rRNA
GAPDH	F: GGTGAAGGTGCGGTGTGAACG R: CTCGCTCCTGGAAGATGGTG	Glyceraldehyde-3-phosphate dehydrogenase
STING	F: CTACATTGGGTACTTGCGGTT R: GCACCACTGAGCATGTTGTATG	Stimulator of interferon genes
TNF- $\alpha$	F: TCCCCAAAGGGATGAGAAG R: CACTTGGTGGTTTGCTACGA	Tumor necrosis factor- $\alpha$
IL-6	F: ACAAGCCAGAGTCTTCAGAGAG R: TTGGATGGTCTTGGTCCCTAGCCA	Interleukin-6
MCP-1	F: TTAAAAACCTGGATCGGAACCAA R: GCATTAGCTTCAGATTTACGGGT	Chemokine (C-C motif) ligand 2
IL-1 $\beta$	F: ACTGTGAAATGCCACCTTTTG R: TGTGTGATGTGCTGCTGTGAG	Interleukin-12b
IL-12b	F: AGGTGCGTTCTCTCGTAGAGA R: AAAGCCAACCAAGCAGAAGA	Interleukin-1 $\beta$
<i>Human</i>		
mt-ND1	F: ATACCCATGGCCAACCTCCT R: GGGCCTTTGCGTAGTTGTAT	NADH dehydrogenase 1, mitochondrial
mt-CO3	F: ATGACCCACCAATCACATGC R: ATCACATGGCTAGGCCGGAG	Cytochrome c oxidase III, mitochondrial
mt-CYTB	F: ATGACCCCAATACGCAAAAT R: CGAAGTTTCATCATGCGGAG	Cytochrome b, mitochondrial

F, forward; R, reverse.

Mitochondrial genome (mtDNA) content was detected by qRT-PCR using specific primers for mt-ND1 and mt-CO1 and analyzed using the  $\Delta C_t$  method as normalized to nuclear DNA content, which was represented by a specific locus on mouse chromosome 6 (24).

### Western Blot Analysis

Western blot analysis was performed to detect protein expression in kidney tissues. In brief, frozen kidneys were lysed using protein lysis buffer (50 mM Tris, 150 mM NaCl, 10 mM EDTA, 1% Triton X-100, and 200 mM sodium fluoride supplemented with 1× protease inhibitor cocktail, ThermoFisher Scientific, Waltham, MA). Proteins from the tissues were separated by SDS-PAGE, transferred to polyvinylidene difluoride (PVDF) membranes, and then incubated with antibodies against the protein of interest, including STING (Cat. No. 19851-1-AP, Protein-tech), neutrophil gelatinase-associated lipocalin (Cat. No. ab63929, Abcam, Cambridge, UK), cleaved caspase-3 (Cat. No. 9664, Cell Signaling Technology), and  $\beta$ -actin (Cat. No. AP0060, Bioworld) followed by an incubation with horseradish peroxidase-labeled secondary antibodies (Beyotime, Shanghai, China). Blots were visualized using ECL Plus Western blotting detection reagents (Millipore, Bedford, MA). Protein quantification was analyzed by measuring the density of band using ImageJ software and was normalized to the expression of  $\beta$ -actin.

### ELISA

The level of IL-6 in plasma was measured by ELISA kits (Cat. No. 12-2060, Dakewe Biotech, Beijing, China). In brief,

blood was collected from the postcaval ureter of anesthetized mice using anticoagulant tubes and centrifuged at 3,000 rpm. The obtained plasma samples were analyzed for IL-6 according to the manufacturer's instructions.

### TUNEL Staining

For apoptosis assay, TUNEL staining was performed on paraffin-fixed kidney sections to detect in situ cell death according to the manufacturer's instruction (Cat. No. A112-01/02/03, Vazyme). Sections were examined under microscopy, and images were acquired by laser scanning confocal microscopy (LSM710, Carl Zeiss). Five randomly visual fields of blinded samples were checked, and the number of apoptotic cells was counted.

### Statistical Analysis

Data were analyzed using GraphPad Prism 7 software and presented as means  $\pm$  SE. Statistical analyses were performed using a Student's *t* test or ANOVA followed by Bonferroni's comparison test. *P* values of  $<0.05$  were considered significant.

## RESULTS

### STING Expression Was Increased in the Kidneys of Cisplatin-Treated Mice

First, we examined the expression of STING in kidney tissues from cisplatin-treated mice. As shown in Fig. 1, cisplatin noteworthy increased STING expression at both mRNA (Fig. 1D) and protein levels (Fig. 1, A–C), suggesting an activation of renal STING in cisplatin-induced AKI.

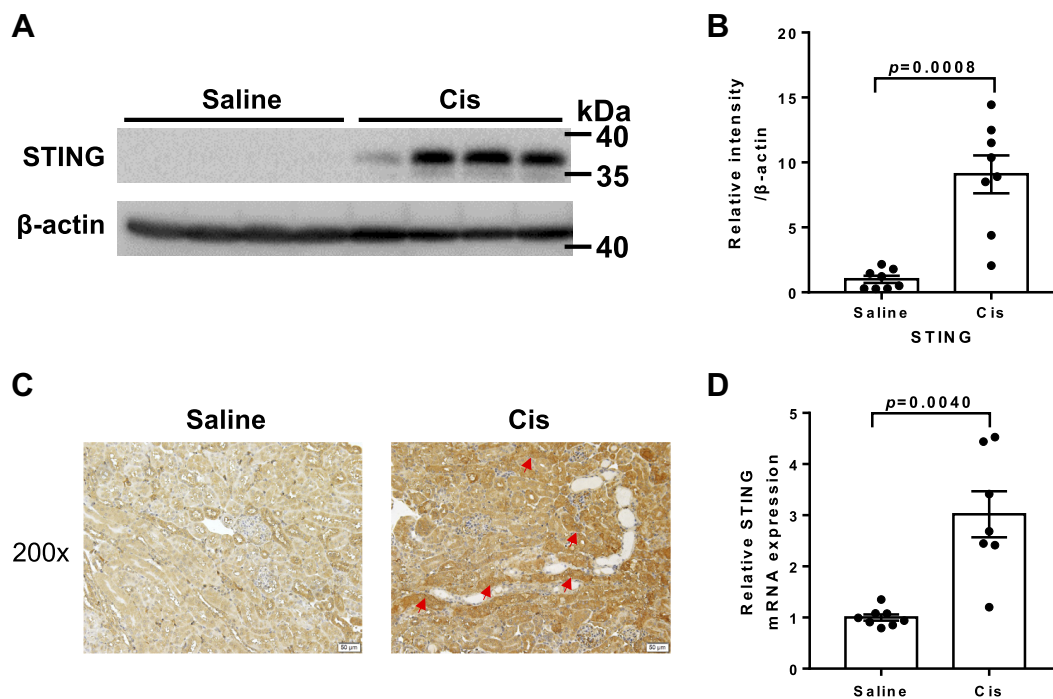


**Figure 1.** Stimulator of interferon genes (STING) expression in renal tissues from cisplatin (Cis)-treated mice. **A:** representative blots of STING. **B:** relative densitometry of STING normalized to  $\beta$ -actin ( $n = 8$ ). **C:** STING immunohistochemistry staining in renal tissues. Arrows indicate the increased staining of STING in tubules. Scale bars = 50  $\mu$ m. **D:** quantitative RT-PCR analysis of STING mRNA levels in renal tissues ( $n = 7$ –8). Data are shown as means  $\pm$  SE. *P* values of  $<0.05$  were considered significant.



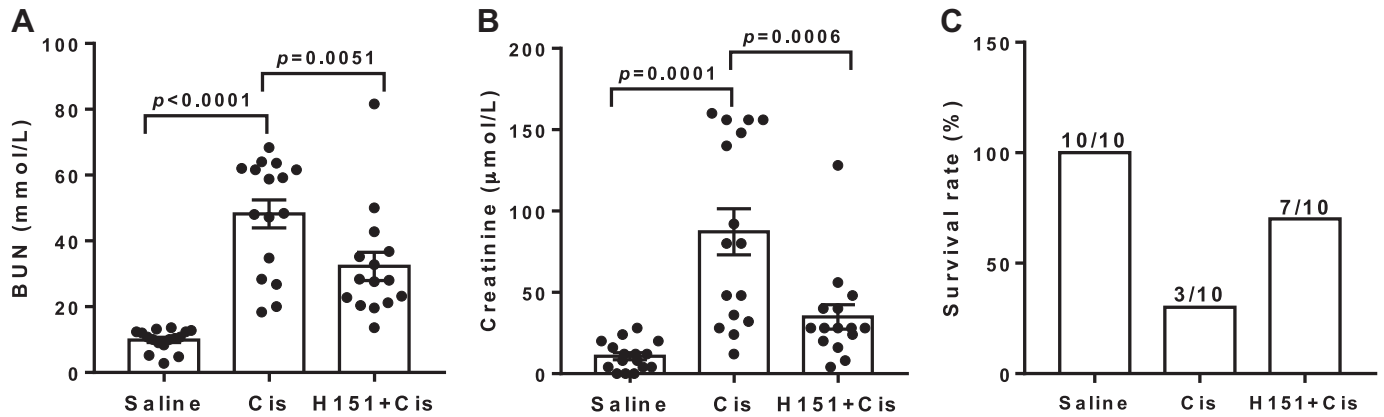


**Figure 2.** H151 alleviated renal dysfunction and survival induced by cisplatin (Cis). Mouse plasma from different groups ( $n=16-17$ ) was collected, and blood urea nitrogen (BUN; A) and creatinine (B) were measured by the biochemical autoanalyzer. C: survival rate was monitored at 96 h after cisplatin treatment ( $n=10$ ). Data are shown as means  $\pm$  SE.  $P$  values of  $<0.05$  were considered significant.

### H151 Improved Renal Function and Survival in Mice With Cisplatin-Induced AKI

H151, the specific inhibitor of STING, was used to explore the effect on cisplatin-induced AKI in mice. Figure 2, A and B, shows that H151 treatment significantly reduced the levels of BUN and creatinine in cisplatin-treated mice. Furthermore, we detected the effect of H151 on the survival rate at 96 h after cisplatin challenge. As shown in Fig. 2C, H151 treatment improved the survival rate of cisplatin-treated mice from 30% to 70%. These data indicated that H151 protected against cisplatin-induced renal dysfunction.

### H151 Attenuated Renal Tubular Injury and Cell Apoptosis in Cisplatin-Induced AKI

Hematoxylin and eosin staining of kidneys revealed severe tubular dilation, tubular necrosis, and cast formation

in cisplatin-treated mice, which was strikingly ameliorated in H151-treated mice (Fig. 3A). Semiquantitative analysis of the tubular injury score confirmed the significant difference (Fig. 3B). Furthermore, neutrophil gelatinase-associated lipocalin, an early biomarker of renal tubular damage, was decreased in H151-treated animals compared with animals with cisplatin-alone treatment (Fig. 3, C and D).

Apoptosis of renal tubular cells is a major feature of cisplatin-induced AKI and strong evidence for tubular damage. Kidney tissues from cisplatin-treated mice showed obvious apoptotic tubular cells stained with TUNEL, while H151 treatment reduced the number of TUNEL-positive cells (Fig. 4, A and B). These data were consistent with the decreased level of cleaved caspase-3 in kidney tissues from the H151-treated group (Fig. 4, C and D), suggesting that H151 ameliorated cisplatin-induced renal tubular cell death in mice.

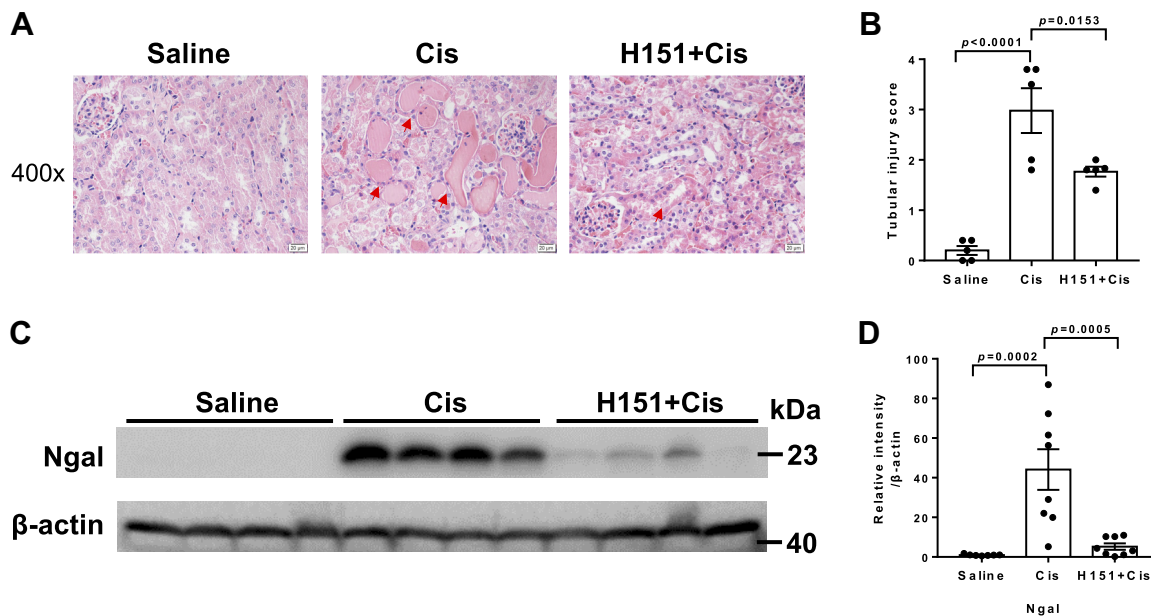


**Figure 3.** H151 alleviated renal tubular injury induced by cisplatin (Cis). A: representative images of hematoxylin and eosin staining. Arrows indicate injured tubes. Scale bars = 20  $\mu$ m. B: tubular injury scores in mice were analyzed ( $n=5$ ). C: representative blots of neutrophil gelatinase-associated lipocalin (Ngal). D: relative densitometry of Ngal normalized to  $\beta$ -actin ( $n=7-8$ ). Data are shown as means  $\pm$  SE.  $P$  values of  $<0.05$  were considered significant.

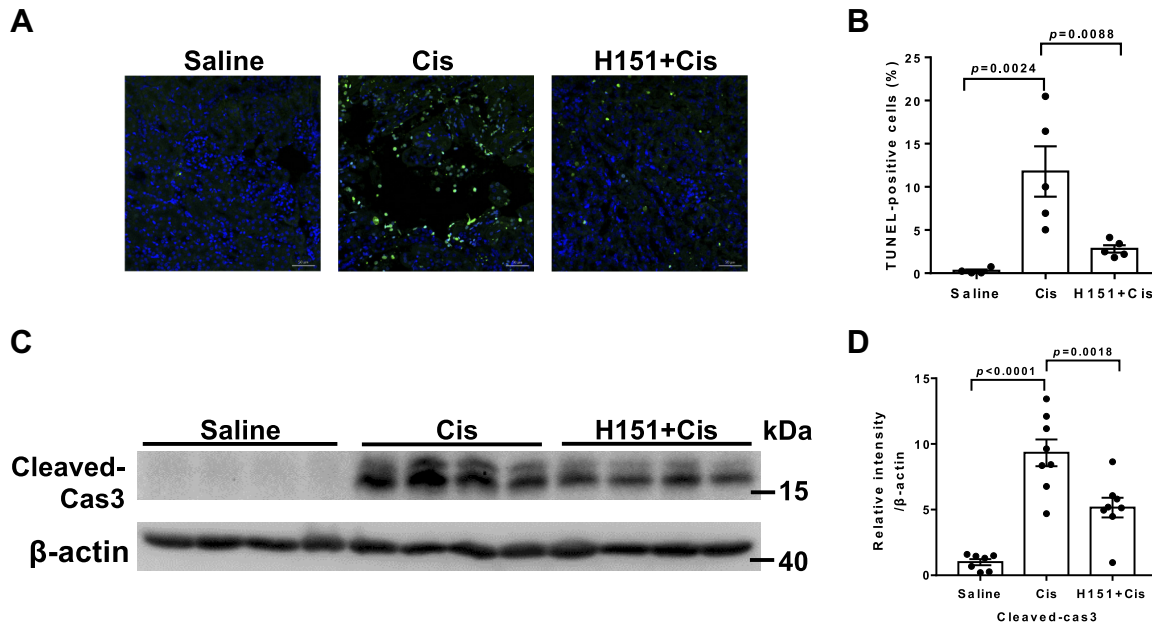


**Figure 4.** H151 alleviated apoptosis of renal tubular cells induced by cisplatin (Cis). **A:** representative images of TUNEL. Scale bars = 50  $\mu$ m. **B:** quantification of TUNEL-positive cells ( $n=4-5$ ). **C:** representative blots of cleaved caspase-3 (cleaved-cas3). **D:** relative densitometry of cleaved caspase-3 normalized to  $\beta$ -actin ( $n=7-8$ ). Data are shown as means  $\pm$  SE.  $P$  values of  $<0.05$  were considered significant.

### H151 Suppressed Renal Inflammation Induced by Cisplatin

To examine the effect of H151 on inflammatory cytokine production in cisplatin-challenged mice, we analyzed the inflammatory cytokine IL-6 in the plasma and inflammatory factors in kidney tissues. **Figure 5** shows that H151 treatment significantly decreased IL-6 in the circulation (**Fig. 5A**), and mRNA expression of inflammatory factors, such as TNF- $\alpha$ , IL-6, monocyte chemoattractant protein-1, IL-1 $\beta$ , and IL-12b, were also reduced in kidney tissues from H151-treated mice (**Fig. 5B**), indicating an anti-inflammatory effect of H151 on cisplatin-induced AKI.

### H151 Improved Renal Mitochondrial Injury in Cisplatin-Treated Mice

Mitochondrial dysfunction of tubular cells is a crucial pathogenic factor in cisplatin nephrotoxicity. Ameliorating mitochondrial dysfunction has supposed to be an effective therapy for AKI. Here, we tested the mitochondrial status of renal tubules in cisplatin-treated mice. Strikingly, the reduced expression of multiple mitochondria-encoded genes in the kidneys of cisplatin-treated mice was largely reversed after H151 administration (**Fig. 6A**). Consistently, the decreased mtDNA content in kidneys was reversed by H151 treatment (**Fig. 6B**). In addition, we performed electron microscopical analysis and found severe mitochondrial structure damage in

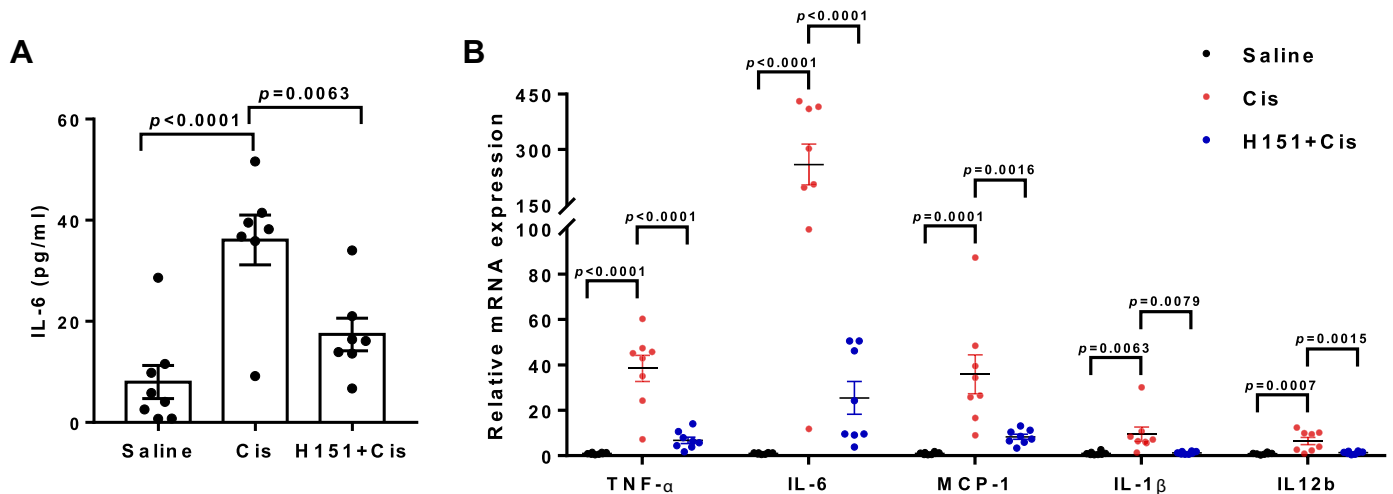


**Figure 5.** H151 inhibited renal inflammation induced by cisplatin (Cis). **A:** plasma levels of IL-6 ( $n=7-8$ ). **B:** quantitative RT-PCR analysis of tumor necrosis factor (TNF)- $\alpha$ , interleukin (IL)-6, monocyte chemoattractant protein (MCP)-1, IL-1 $\beta$ , and IL-12b mRNA from renal tissues ( $n=8$ ). Data are shown as means  $\pm$  SE.  $P$  values of  $<0.05$  were considered significant.

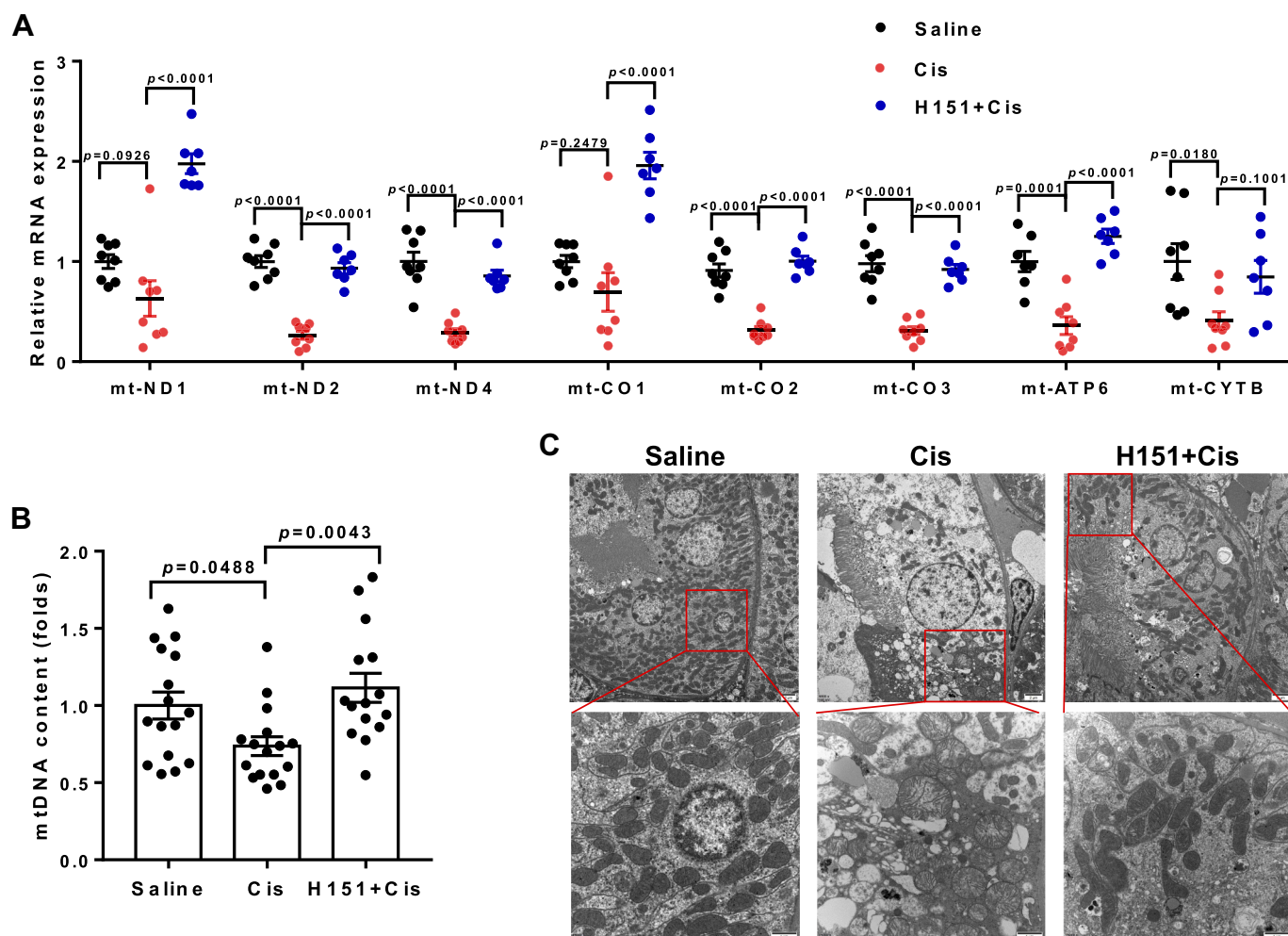


**Figure 6.** H151 improved mitochondrial injury in cisplatin (Cis)-treated mice. **A:** mRNA expression of multiple genes encoded by the mitochondrial genome ( $n=7-8$ ). **B:** mtDNA content of renal tissues as assessed by quantitative RT-PCR ( $n=7-8$ ). Dots show the results from two pairs of primers [mitochondrially encoded NADH:ubiquinone oxidoreductase core subunit 1 (mt-ND1) and mitochondrially encoded cytochrome *c* oxidase I (mt-CO1)]. **C:** representative electron micrographs of renal tubular mitochondria. Scale bars = 2  $\mu$ m (top lines) and 1  $\mu$ m (enlarged sections), respectively. Data are shown as means  $\pm$  SE. *P* values of  $<0.05$  were considered significant. mt-ND2 and mt-ND4, mitochondrially encoded NADH:ubiquinone oxidoreductase core subunits 1 and 4, respectively; mt-CO2 and mt-CO3, mitochondrially encoded cytochrome *c* oxidase II and III, respectively; mt-ATP6, mitochondrially encoded ATP synthase membrane subunit 6; mt-CYTb, mitochondrially encoded cytochrome *b*.

renal tubular cells of the cisplatin-alone group, while such an abnormality was obviously improved in the H151-treated group (Fig. 6C). These data indicated that H151 treatment attenuated mitochondrial impairment of tubular cells in cisplatin-induced AKI.

#### Analysis of mtDNA Levels in the Plasma of Patients Receiving Platinum-Based Chemotherapy

Eight blood samples from patients with platinum-based chemotherapy and nine normal controls were collected for the

analysis of mtDNA levels in plasma. Plasma mtDNA concentration was quantified using qRT-PCR and expressed as  $C_t$  values by amplifying the mitochondrial genomic regions of mt-ND1, mt-CO3, and mt-CYTb, respectively. As shown in Table 3, all  $C_t$  values for plasma samples were below 40, which meant an effective detection for mtDNA (20). The mtDNA concentration, which was quantified as  $C_t$  values for three selected sequences in patients with platinum-based chemotherapy, was significantly higher than that of normal subjects, suggesting that cisplatin treatment may cause mtDNA release.

**Table 3.** Plasma mtDNA levels in patients with platinum-based chemotherapy and controls

mtDNA	Control $C_t$ ( $n=9$ )	Patients with Platinum-Based Chemotherapy $C_t$ ( $n=8$ )	<i>P</i> Value
mt-ND1	21.62 $\pm$ 0.3603	19.92 $\pm$ 0.3221	0.0034
mt-CO3	22.09 $\pm$ 0.3324	20.46 $\pm$ 0.3021	0.0027
mt-CYTb	21.72 $\pm$ 0.3714	19.84 $\pm$ 0.3178	0.0017

$C_t$ , threshold cycle; mt-CO3, cytochrome *c* oxidase III, mitochondrial; mt-CYTb, cytochrome *b*, mitochondrial; mt-ND1, NADH dehydrogenase 1, mitochondrial.



## DISCUSSION

mtDNA released from damaged mitochondria is a marker of renal dysfunction and disease progression in AKI based on the evidences from both animal and human studies. The level of mtDNA in urine was positively correlated with the levels of serum creatinine and BUN and negatively correlated with the glomerular filter rate (25–28). In addition, mtDNA from damaged tubular cells could serve as a ligand to activate STING and downstream signals and thus trigger renal tubular inflammation in AKI (4). Studies have suggested that STING participates in renal tubular inflammation and injury in AKI, and targeting STING might be an effective therapy for the treatment of AKI. However, the effect of STING inhibitors targeting human STING on AKI has not been tested. Here, we report that H151, a specific antagonist of STING targeting both human and murine STING, was useful to protect against cisplatin-induced AKI, as evidenced by the improvement of renal function, kidney morphology, renal inflammation, and mitochondrial injury, thus providing a potential agent for treating AKI.

STING-mediated pathways are important parts of the innate immune system that mainly participate in the defense of invading pathogens (29). In recent years, STING has captured more and more attention as a crucial regulator in infection, tumor, autoimmune diseases, and inflammatory diseases. STING agonists are being tested in cancer therapies because of the rationale that STING activity could trigger an immunostimulatory response that controls tumor escape (30). Moreover, STING inhibitors are used to treat autoimmune or autoinflammatory diseases in experimental models for their effect on the innate inflammatory response (31). However, the clinical translation of molecules targeting STING is still a tough challenge for the species-based limitation between human STING and mouse STING (32, 33). For example, vadimezan, a specific agonist for STING, was suspended in clinical testing because it binds only to mouse STING (30, 34). Therefore, it is of importance to screen compounds targeting human STING.

H151 is a selective small-molecule antagonist of STING that was identified using a human cell-based screening system. A study has shown that H151 could inhibit human STING with a more advanced effect and low background reactivity in human embryonic kidney-293 cells. Interestingly, H151 also has good bioactivity in mice, providing a possibility of being able to translate into clinical studies when it displays effective treatment in murine disease models (19). Since our data indicated a renoprotective effect of H151 in a mouse model of cisplatin-induced AKI, it is reasonable to speculate a possibility of H151 for becoming a drug in clinical research. Another recent study also used another STING inhibitor, C-176, to treat the AKI mouse model and showed beneficial effects including reduced renal inflammation and attenuated tubular injury and renal dysfunction (4). In fact, C-176 is a covalent antagonist of STING that had the same covalent site as H151, but, unfortunately, C-176 mainly inhibited mouse STING and had limited binding activity with human STING, which limited the implication of C-176 in clinical trials (19).

Mitochondrial dysfunction is considered as an early event of AKI and a contributor to acute renal tubular injury. Strategies improving mitochondrial functions have been demonstrated to be beneficial for AKI treatment in mice

models (35, 36). In renal tubular epithelial cells of AKI mice, the mitochondria membrane potential was decreased and mtDNA was released into the cytoplasm (4). Free mtDNA induced STING pathways and thus implicated tubular cell injury (4, 10). Interestingly, our results indicated that H151 could ameliorate renal tubular mitochondrial damage, as shown by the improved mitochondrial morphology and restored mtDNA content and mitochondrial gene expression. The improvement of mitochondrial dysfunction could block further release of mtDNA and therefore suppress STING signal-mediated inflammation and apoptosis.

However, some limitations of this study should be noted. First, we did not evaluate the effect of H151 on AKI in STING knockout mice *in vivo*. Thus, the *in vivo* evidence for the specificity of H151 on STING-dependent renal injury needs further study. Second, we did not observe the effect of H151 on tumor growth, which could limit the understanding of the effect of H151 on tumor pathology in clinical studies. Finally, the number of patients enrolled in this study was relatively small. Further assessment of plasma mtDNA in a larger population of patients with platinum-based chemotherapy is required.

In summary, this study explored the effect of the human/murine STING inhibitor H151 against cisplatin-induced AKI and found a protective effect of H151 on kidney function, renal tubular cell injury, and mitochondrial dysfunction. Our findings suggest a translational potential of H151 in the treatment of cisplatin-induced human AKI.

## GRANTS

This work was supported by National Key Research and Development Program Grant 2016YFC0906103; National Natural Science Foundation of China Grants 81970581, 81700595, and 82070701; and Nanjing Medical Science and Technique Development Foundation Grant QRX17166.

## DISCLOSURES

No conflicts of interest, financial or otherwise, are declared by the authors.

## AUTHOR CONTRIBUTIONS

W.G., A.Z., and Z.J. conceived and designed research; W.G., L.L., Y. Zhou, J.L., H.M., and L.F. performed experiments; W.G., L.L., and Y. Zhou analyzed data; W.G., S.H., Y. Zhang, A.Z., and Z.J. interpreted results of experiments; W.G. prepared figures; W.G. and Z.J. drafted manuscript; W.G., Y. Zhang, and Z.J. edited and revised manuscript; W.G., L.L., Y. Zhou, S.H., Y. Zhang, A.Z., and Z.J. approved final version of manuscript.

## REFERENCES

1. Briggs DL. Disparities in health outcomes with dialysis in the United States vary by race. *Clin J Am Soc Nephrol* 15: 1, 2020. doi:10.2215/CJN.13881119.
2. Duann P, Lianos EA, Ma J, Lin P-H. Autophagy innate immunity and tissue repair in acute kidney injury. *Int J Mol Sci* 17: 662, 2016. doi:10.3390/ijms17050662.
3. He L, Wei Q, Liu J, Yi M, Liu Y, Liu H, Sun L, Peng Y, Liu F, Venkatachalam MA, Dong Z. AKI on CKD: heightened injury, suppressed repair, and the underlying mechanisms. *Kidney Int* 92: 1071–1083, 2017. doi:10.1016/j.kint.2017.06.030.
4. Maekawa H, Inoue T, Ouchi H, Jao T-M, Inoue R, Nishi H, Fujii R, Ishidate F, Tanaka T, Tanaka Y, Hirokawa N, Nangaku M, Inagi R.



- Mitochondrial damage causes inflammation via cGAS-STING signaling in acute kidney injury. *Cell Rep* 29: 1261–1273.e6, 2019. doi:10.1016/j.celrep.2019.09.050.
5. Ablasser A, Chen ZJ. cGAS in action: expanding roles in immunity and inflammation. *Science* 363: eaat8657, 2019. doi:10.1126/science.aat8657.
  6. Sun L, Wu J, Du F, Chen X, Chen ZJ. Cyclic GMP-AMP synthase is a cytosolic DNA sensor that activates the type I interferon pathway. *Science* 339: 786–791, 2013. doi:10.1126/science.1232458.
  7. Zhang C, Shang G, Gui X, Zhang X, Bai XC, Chen ZJ. Structural basis of STING binding with and phosphorylation by TBK1. *Nature* 567: 394–398, 2019. doi:10.1038/s41586-019-1000-2.
  8. Zhang X, Bai X-C, Chen ZJ. Structures and mechanisms in the cGAS-STING innate immunity pathway. *Immunity* 53: 43–53, 2020. doi:10.1016/j.immuni.2020.05.013.
  9. Benmerzoug S, Rose S, Bounab B, Gosset D, Duneau L, Chenuet P, Mollet L, Le Bert M, Lambers C, Geleff S, Roth M, Fauconnier L, Sedda D, Carvalho C, Perche O, Laurenceau D, Ryffel B, Apetoh L, Kiziltunc A, Uslu H, Albez FS, Akgun M, Togbe D, Quesniaux VFJ. STING-dependent sensing of self-DNA drives silica-induced lung inflammation. *Nat Commun* 9: 5226, 2018. doi:10.1038/s41467-018-07425-1.
  10. Chung KW, Dhillon P, Huang S, Sheng X, Shrestha R, Qiu C, Kaufman BA, Park J, Pei L, Baur J, Palmer M, Susztak K. Mitochondrial damage and activation of the STING pathway lead to renal inflammation and fibrosis. *Cell Metab* 30: 784–799.e5, 2019. doi:10.1016/j.cmet.2019.08.003.
  11. Yu Y, Liu Y, An W, Song J, Zhang Y, Zhao X. STING-mediated inflammation in Kupffer cells contributes to progression of nonalcoholic steatohepatitis. *J Clin Invest* 129: 546–555, 2019. doi:10.1172/JCI121842.
  12. Long J, Yang C, Zheng Y, Loughran P, Guang F, Li Y, Liao H, Scott M, Tang D, Billiar T, Deng M. Notch signaling protects CD4 T cells from STING-mediated apoptosis during acute systemic inflammation. *Sci Adv* 6: eabc5447, 2020. doi:10.1126/sciadv.abc5447.
  13. Murayama G, Chiba A, Kuga T, Makiyama A, Yamaji K, Tamura N, Miyake S. Inhibition of mTOR suppresses IFN $\alpha$  production and the STING pathway in monocytes from systemic lupus erythematosus patients. *Rheumatology (Oxford)* 59: 2992–3002, 2020. doi:10.1093/rheumatology/keaa060.
  14. Reinert L, Rashidi A, Tran D, Katzilleris-Petras G, Hvidt A, Gohr M, Fruhwürth S, Bodda C, Thomsen M, Vendelbo M, Khan A, Hansen B, Bergström P, Agholme L, Mogensen T, Christensen M, Nyengaard J, Sen G, Zetterberg H, Verjans G, Paluden S. Brain immune cells undergo cGAS-STING-dependent apoptosis during herpes simplex virus type 1 infection to limit type I IFN production. *J Clin Invest* 131: e136824, 2021. doi:10.1172/JCI136824.
  15. Saldanha R, Balka K, Davidson S, Wainstein B, Wong M, Macintosh R, Loo C, Weber M, Kamath V, Moghaddas F, De Nardo D, Gray P, Masters S; AADRY. A mutation outside the dimerization domain causing atypical STING-associated vasculopathy with onset in infancy. *Front Immunol* 9: 1535, 2018. doi:10.3389/fimmu.2018.01535.
  16. Wang L, Yang L, Wang C, Zhao W, Ju Z, Zhang W, Shen J, Peng Y, An C, Luu Y, Song S, Yap T, Ajani J, Mills G, Shen X, Peng G. Inhibition of the ATM/Chk2 axis promotes cGAS-STING signaling in ARID1A-deficient tumors. *J Clin Invest* 130: 5951–5966, 2020. doi:10.1172/JCI130445.
  17. Canesso MCC, Lemos L, Neves TC, Marim FM, Castro TBR, Veloso ES, Queiroz CP, Ahn J, Santiago HC, Martins FS, Alves-Silva J, Ferreira E, Cara DC, Vieira AT, Barber GN, Oliveira SC, Faria AMC. The cytosolic sensor STING is required for intestinal homeostasis and control of inflammation. *Mucosal Immunol* 11: 820–834, 2018. doi:10.1038/s41385-017-88.
  18. Zhang H, Zeng L, Xie M, Liu J, Zhou B, Wu R, Cao L, Kroemer G, Wang H, Billiar TR, Zeh HJ, Kang R, Jiang J, Yu Y, Tang D. TMEM173 drives lethal coagulation in sepsis. *Cell Host Microbe* 27: 556–570.e6, 2020. doi:10.1016/j.chom.2020.02.004.
  19. Haag SM, Gulen MF, Reymond L, Gibelin A, Abrami L, Decout A, Heymann M, van der Goot FG, Turcatti G, Behrendt R, Ablasser A. Targeting STING with covalent small-molecule inhibitors. *Nature* 559: 269–273, 2018. doi:10.1038/s41586-018-0287-8.
  20. Hu Q, Ren J, Wu J, Li G, Wu X, Liu S, Wang G, Gu G, Li J. Elevated levels of plasma mitochondrial DNA are associated with clinical outcome in intra-abdominal infections caused by severe trauma. *Surg Infect (Larchmt)* 18: 610–618, 2017. doi:10.1089/sur.2016.276.
  21. You R, Zhou W, Li Y, Zhang Y, Huang S, Jia Z, Zhang A. Inhibition of ROCK2 alleviates renal fibrosis and the metabolic disorders in the proximal tubular epithelial cells. *Clin Sci (Lond)* 134: 1357–1376, 2020. doi:10.1042/CS20200030.
  22. Yang Y, Liu S, Gao H, Wang P, Zhang Y, Zhang A, Jia Z, Huang S. Ursodeoxycholic acid protects against cisplatin-induced acute kidney injury and mitochondrial dysfunction through acting on ALDH1L2. *Free Radic Biol Med* 152: 821–837, 2020. doi:10.1016/j.freeradbiomed.2020.01.182.
  23. Bai M, Chen H, Ding D, Song R, Lin J, Zhang Y, Guo Y, Chen S, Ding G, Zhang Y, Jia Z, Huang S, He JC, Yang L, Zhang A. MicroRNA-214 promotes chronic kidney disease by disrupting mitochondrial oxidative phosphorylation. *Kidney Int* 95: 1389–1404, 2019. doi:10.1016/j.kint.2018.12.028.
  24. Liao X, Zhang R, Lu Y, Prosdocimo DA, Sangwung P, Zhang L, Zhou G, Anand P, Lai L, Leone TC, Fujioka H, Ye F, Rosca MG, Hoppel CL, Schulze PC, Abel ED, Stamler JS, Kelly DP, Jain MK. Kruppel-like factor 4 is critical for transcriptional control of cardiac mitochondrial homeostasis. *J Clin Invest* 125: 3461–3476, 2015. doi:10.1172/JCI79964.
  25. Hu Q, Ren J, Ren H, Wu J, Wu X, Liu S, Wang G, Gu G, Guo K, Li J. Urinary mitochondrial DNA identifies renal dysfunction and mitochondrial damage in sepsis-induced acute kidney injury. *Oxid Med Cell Longev* 2018: 8074936, 2018. doi:10.1155/2018/8074936.
  26. Hu Q, Ren J, Wu J, Li G, Wu X, Liu S, Wang G, Gu G, Ren H, Hong Z, Li J. Urinary mitochondrial DNA levels identify acute kidney injury in surgical critical illness patients. *Shock* 48: 11–17, 2017. doi:10.1097/SHK.0000000000000830.
  27. Jansen MPB, Pulskens WP, Butter LM, Florquin S, Juffermans NP, Roelofs J, Leemans JC. Mitochondrial DNA is released in urine of SIRS patients with acute kidney injury and correlates with severity of renal dysfunction. *Shock* 49: 301–310, 2018. doi:10.1097/SHK.0000000000000967.
  28. Whitaker RM, Stallons LJ, Kneff JE, Alge JL, Harmon JL, Rahn JJ, Arthur JM, Beeson CC, Chan SL, Schnellmann RG. Urinary mitochondrial DNA is a biomarker of mitochondrial disruption and renal dysfunction in acute kidney injury. *Kidney Int* 88: 1336–1344, 2015. doi:10.1038/ki.2015.240.
  29. Abe T, Harashima A, Xia T, Konno H, Konno K, Morales A, Ahn J, Gutman D, Barber GN. STING recognition of cytoplasmic DNA instigates cellular defense. *Mol Cell* 50: 5–15, 2013. doi:10.1016/j.molcel.2013.01.039.
  30. Le Naour J, Zitvogel L, Galluzzi L, Vacchelli E, Kroemer G. Trial watch: STING agonists in cancer therapy. *Oncoimmunology* 9: 1777624, 2020. doi:10.1080/2162402X.2020.1777624.
  31. Li S, Hong Z, Wang Z, Li F, Mei J, Huang L, Lou X, Zhao S, Song L, Chen W, Wang Q, Liu H, Cai Y, Yu H, Xu H, Zeng G, Wang Q, Zhu J, Liu X, Tan N, Wang C. The cyclopeptide astin C specifically inhibits the innate immune CDN sensor STING. *Cell Rep* 25: 3405–3421, 2018. e3407 doi:10.1016/j.celrep.2018.11.097.
  32. Cavar T, Deimling T, Ablasser A, Hopfner KP, Hornung V. Species-specific detection of the antiviral small-molecule compound CMA by STING. *EMBO J* 32: 1440–1450, 2013. doi:10.1038/emboj.2013.86.
  33. Ergun SL, Fernandez D, Weiss TM, Li L. STING polymer structure reveals mechanisms for activation, hyperactivation, and inhibition. *Cell* 178: 290–301.e10, 2019. doi:10.1016/j.cell.2019.05.036.
  34. Conlon J, Burdette DL, Sharma S, Bhat N, Thompson M, Jiang Z, Rathnam VA, Monks B, Jin T, Xiao TS, Vogel SN, Vance RE, Fitzgerald KA. Mouse, but not human STING, binds and signals in response to the vascular disrupting agent 5,6-dimethylxanthone-4-acetic acid. *J Immunol* 190: 5216–5225, 2013. doi:10.4049/jimmunol.1300097.
  35. Sun J, Zhang J, Tian J, Virzi GM, Digvijay K, Cueto L, Yin Y, Rosner MH, Ronco C. Mitochondria in sepsis-induced AKI. *J Am Soc Nephrol* 30: 1151–1161, 2019. doi:10.1681/ASN.201811126.
  36. Zhao L, Hu C, Zhang P, Jiang H, Chen J. Mesenchymal stem cell therapy targeting mitochondrial dysfunction in acute kidney injury. *J Transl Med* 17: 142, 2019. doi:10.1186/s12967-019-1893-4.